J Mater Sci: Mater Med (2014) 25:2677–2689
DOI 10.1007/s10856-014-5286-1

Effect of surfactant types on the biocompatibility of electrospun HAp/PHBV composite nanofibers

A. Suslu · A. Z. Albayrak · A. S. Urkmez · E. Bayir · U. Cocen

Received: 1 November 2013 / Accepted: 21 July 2014 / Published online: 5 August 2014

Abstract Bone tissue engineering literature conveys investigations regarding biodegradable polymers where bioactive inorganic materials are added either before or after electrospinning process. The goal is to mimic the composition of bone and enhance the biocompatibility of the materials. Yet, most polymeric materials are hydrophobic in nature; therefore, their surfaces are not favorable for human cellular adhesion. In this sense, modifications of the hydrophobic surface of electrospun polymer fibers with hydrophilic and bioactive nanoparticles are beneficial. In this work, dispersion of hydroxyapatite (HAp), which is similar to the mineral component of natural bone, within biodegradable and biocompatible polymer poly(3-hydroxybutyrate-co-3-hydroxyvalerate) (PHBV) with the aid of a surfactant has been investigated. Non-ionic TWEEN20 and 12-hydroxysteric acid (HSA), cationic dodecyl trimethyl ammonium bromide (DTAB) and anionic sodium deoxycholate and sodium dodecyl sulfate (SDS) surfactants were used for comparison in order to prepare stable and homogenous nanocomposite suspensions of HAp/PHBV for the electrospinning process. Continuous and uniform composite nanofibers were generated successfully within a diameter range of 400–1,000 nm by the mediation of all surfactant types. Results showed that incorporation of HAp and any of the surfactant types strongly activates the precipitation rate of the apatite-like particles and decreases percent crystallinity of the HAp/PHBV mats. Mineralization was greatly enhanced on the fibers produced by using DTAB, HSA, and especially SDS on where also osteoblastic metabolic activity was similarly increased. The produced HAp/PHBV nanofibrous composite scaffolds would be a promising candidate as an osteoconductive bioceramic/polymer composite material for tissue engineering applications.

A. Suslu · A. Z. Albayrak (✉) · U. Cocen
Metallurgical and Materials Engineering Department, Dokuz Eylul University, Izmir, Turkey
e-mail: aylin.albayrak@deu.edu.tr

A. Suslu
The Graduate School of Natural and Applied Sciences, Dokuz Eylul University, Izmir, Turkey

A. S. Urkmez · E. Bayir
Bioengineering Department, Ege University, Izmir, Turkey

1 Introduction

Bone tissue engineering has gained significant interest over the last decade since it offers a new and promising approach for bone repair and regeneration. A range of new materials and a variety of processing techniques have been developed to mimic bone extracellular matrix (ECM) for potential applications as tissue engineering scaffolds [1]. Therefore, it is important to design materials with structure, composition and properties similar to bone ECM [1, 2]. An ideal scaffold should support cell attachment, proliferation and differentiation while providing a porous network for cell nutrients and cellular waste products transport and tissue in growth [3, 4]. Its degradation rate should match the rate of new tissue formation and both the degradation products and the scaffold itself must be biocompatible. Also, the scaffold should have sufficient mechanical properties so as to provide structural support for the new tissue formation [5, 6]. The bone ECM is a type of organic–inorganic nanocomposite composed mainly of organic collagenous fibers within which inorganic HAp nanocrystals are embedded. Hence the approach of using inorganic materials with the aim of achieving both bone-specific

biofunctionality and mechanical properties with biodegradable organic polymers has attracted much attention in developing synthetic ECM matrices [1, 3, 7–9]. Three different methods have been used in the production of nanofibrous scaffolds for tissue engineering; electrospinning, self-assembly and phase separation [10–15]. Among these, electrospinning is considered as the simplest and cheapest way of generating nanofibrous scaffolds. Above all, electrospinning has received significant attention because of the structural similarity of the nanofibrous matrices fabricated to collagenous ECM [5, 16, 17]. However, it should be remarked that electrospinning of organic–inorganic compounds requires special attention in terms of solution preparation since incorporating inorganic particles in a polymer matrix brings about processing and dispersion problems [1, 18, 19]. In order to overcome these difficulties, some alternative methods have been developed by various researchers to produce organic–inorganic composite nanofibers via electrospinning.

Song et al. [8] produced a composite mat composed of collagen and hydroxyapatite (HAp) with a finely tuned experimental procedure using electrospinning method. HAp–collagen nanocomposite solution for the electrospinning was prepared first by mineralizing HAp nanocrystals within collagen matrix then freeze drying the co-precipitated product and finally dissolving it in an organic solvent. The electrospun mat showed a well developed fibrous morphology with a HAp content of up to 20 wt% and favored MC3T3-E1 osteoblastic cells' adhesion and growth. The same group also produced HAp precipitate/gelatin matrix nanocomposites potentially applicable in the field of guided tissue regeneration by using the same procedure [20]. Besides natural polymers, synthetic degradable polymers such as PLA, PCL, and poly(3-hydroxybutyrate-co-3-hydroxyvalerate) (PHBV) have also been used in the electrospinning of composite fibers [21]. However, inorganic nanoparticles tend to agglomerate and cannot be homogenized well in the synthetic polymer solutions due to hydrophobic nature of synthetic degradable polymers compared to hydrophilic natural polymers. In an ordinary, HAp and synthetic polymer blending system, only physical adsorption is achieved between HAp particles and polymer matrix resulting in low mechanical properties [1]. Therefore, interface adhesion of HAp particles and polymer matrix plays a major role in the properties of the organic–inorganic composites. In order to increase the interfacial strength between HAp and synthetic degradable polymer, a variety of methods have been proposed. Hong et al. [22] developed the method of grafting PLLA onto the hydroxyl group of the surface of *n*-HAp particles through a chemical linkage by ring-opening polymerization of L-lactide in the presence of stannous octanoate [$Sn(Oct)_2$] as catalyst. The PLLA-*g*-HAp particles dispersed more uniformly into chloroform than the non-grafted one resulting in PLLA-*g*-HAp/PLLA composites that have better mechanical properties than simple *n*-HAp/PLLA blends. Xu et al. [23] also produced composite fibers consisting of poly(L-lactide)-grafted HAp (PLA-*g*-HAp) nanoparticles and polylactide by electrospinning and determined that at 4 wt% of PLA-*g*-HAp, the nanoparticles dispersed uniformly in the fibers but when the amount of PLA-*g*-HAp increased, the nanoparticles began to aggregate, which caused the deterioration of the mechanical properties of the composite fiber mats. It was also shown that increasing PLA-*g*-HAp content increased the degradation rate of the composite mats due to the enhanced wettability of the composite fibers and the ease of escape of the nanoparticles from the nanofiber surfaces during incubation. Another possible way of incorporating bioactive inorganic nanoparticles evenly within the polymeric matrix is through the introduction of ultrafine particles. For example, Fujihara et al. [24] fabricated guided bone regeneration membranes from PCL–$CaCO_3$ composite nanofibers with two different calcium carbonate ($CaCO_3$) ratios (25 and 75 wt%) by using electrospinning method. Composite fibers containing ultrafine $CaCO_3$ particles with a size of $\sim$40 nm showed good mechanical properties as well as osteoblastic adhesion and growth. Ramakrishna et al. [25] developed PCL/nHAp ($\sim$51 nm)/collagen biocomposite fibrous scaffold, which can provide mechanical support and growth of human fetal osteoblasts for tissue engineering of bone. Kim et al. [26] prevented agglomeration of nanoparticles and bead formation during electrospinning by using ultrafine HAp nanocrystals ($\sim$35 nm in size) obtained by a sol–gel process and introducing a surfactant, 12-hydroxysteric acid (HSA). The surfactant acted as a mediator between the hydrophilic HAp powder and the hydrophobic PLA dissolved in chloroform and caused HAp to remain stable in suspension. Continuous and uniform composite fibers obtained with diameters of $\sim$1–2 μm were shown to promote the osteoblastic cell attachment and proliferation. Ito et al. [27] also proposed an alternative way of producing a composite of HAp with PHBV. First, PHBV nanofibrous film was fabricated by electrospinning and then composited with HAp by soaking in simulated body fluid (SBF). It was observed that HAp mineralization enhanced the hydrophilicity and thus the biodegradation rate of the nanofibrous film whereas no positive effect was observed in terms of COS-7 cell adhesion.

In this study, we present a facile way of preparing stable HAp–PHBV composite suspensions including both an organic salt and a surfactant for electrospinning. PHBV, which is the main matrix, was chosen due to its biodegradability and biocompatibility as well as it has longer degradation time than PLA and PLGA polymers [28]. Also, the ultimate degradation product of PHBV is hydroxybutyric acid which is the normal constituent of human blood [29–31]. Organosoluble salt benzyl triethylammonium

chloride (BTEAC) was used to maintain continuous spinning and uniform composite fibers were produced throughout spinning. However, order and amount of organic salt addition at the suspension preparation stage was highly important, otherwise stability of the composite suspension could be ruined easily. Also, different types of surfactants [neutral surfactants: HSA, TWEEN20; anionic surfactants: sodium dodecyl sulfate (SDS), sodium deoxycholate (DOC); cationic surfactant: dodecyl trimethyl ammonium bromide (DTAB)] were chosen so as to disperse HAp within the PHBV matrix in a homogenous manner as well as to investigate the effects of surfactant types on the surface morphology and crystallinity of the electrospun fibers and on the biomineralization rate of apatite like minerals. Finally, the proliferation and viability of osteoblastic cells on electrospun fibers with the selected surfactants are discussed.

2 Materials and methods

2.1 Materials

PHBV (PHV content 5 wt%), HAp nanopowder (particle size <200 nm), BTEAC and chloroform ($CHCl_3$) were purchased from Sigma-Aldrich. HSA, SDS, TWEEN20, DOC and DTAB were obtained from Alfa Aesar. SaOS-2 human osteoblast cell line was purchased from ATCC, Manassas, VA. USA. Fetal bovine serum (FBS) was obtained from BIOCHROM AG, Germany. L-Glutamine and antibiotic and antimycotic formulation were supplied from Invitrogen Corp., USA. All the chemicals were used as received without further purification. Except specified, all other biomineralization and cell culture media and reagents were purchased from Sigma-Aldrich.

2.2 Production of HAp/PHBV nanofibers

HAp nanopowder and PHBV were used in order to produce bioceramic–biopolymer composite nanofibers. First, one of the surfactants HSA, TWEEN20, DOC, DTAB, or SDS was dissolved in chloroform at 0.2 % w/v, with respect to chloroform concentration. Then, HAp nanopowder (5 % w/v) was added to that solution. Milky dispersion of HAp nanopowder was obtained in chloroform with the aid of the surfactant by using an ultrasonic mixer. Meanwhile, 0.9 g of PHBV including an organosoluble salt BTEAC (2 wt%) was dissolved in 5 mL of chloroform at 50 °C. Finally, dispersed HAp nanopowders were mixed with the PHBV solution at an equal volume. Stirring that continued 2 h at 50 °C was followed by stirring at room temperature until a single-phase suspension was obtained.

For the production of composite nanofibers by electrospinning process, HAp/PHBV suspensions were loaded into a plastic syringe equipped with a 22-gauge stainless steel needle, which was connected to a high positive voltage supply (Gamma High Voltage ES30). Electrospinning parameters used were optimized with respect to our preliminary studies. An aluminum foil collector was placed at a distance of 15 cm below the tip of the needle and the solution was fed at 1.0 mL/h rate using a syringe pump (Top Syringe Pump Top-5300). Nanocomposite fibers were collected by applying a high voltage of 20 kV.

2.3 Biomineralization

The electrospun scaffolds were placed in falcon conical tubes containing 10 mL SBF (pH 7.4) which was prepared according to Kokubo and Takadama [32] and were incubated in a water bath at 37 °C for 5 weeks. SBF solutions were changed every 48 h. After biomineralization, the nanocomposite fibers were washed three times with deionized water to remove residual salts and dried at room temperature before further analysis.

2.4 Cell culture

SaOS-2 cells from a human osteosarcoma cell line with osteoblast-like properties were cultured in McCoy's medium 5A expansion media, supplemented with 15 % FBS, 1 % L-glutamine and 0.1 % penicillin/streptomycin (10,000 units/mL penicillin–10,000 μg/mL streptomycin) at 37 °C in a 5 % CO_2 humidified environment. This cell line has been reported to show characteristics of osteoblastic phenotype and mineralization under these conditions, and has been used as a model osteoblastic cell line for various biomaterials studies [33–35]. After a subconfluent monolayer was achieved, cells were harvested by gentle digestion with 0.05 % trypsin/EDTA, counted with a hemocytometer, and suspended in fresh media before seeding onto scaffolds.

All scaffolds were sterilized both by irradiation ultraviolet (UV) light for 1 h for each surface and by immersion in 70 % ethanol for overnight. After the incubation with ethanol, scaffolds were centrifuged with fresh 70 % ethanol for three times (100 g for 10 min). After hydration through an ethanol series (70–10 %), they were washed with phosphate buffered saline (PBS) three times and conditioned with complete culture medium for 2 h. Scaffolds were drained on sterile gauze to remove excess media and then placed in 96-well culture plates coated with agarose to avoid cell migration onto the plate surface. 25 μL of cell suspension at a density of 1.0×10^4 cells/well was applied dropwise to the top surface of the scaffold which fully absorbed the media, allowing the cells to diffuse throughout the scaffold. After 60 min, 175 μL of

complete culture media were added onto the culture plates. Cells on scaffolds were cultured for up to 14 days in 5 % CO_2, humidified atmosphere at 37 °C and the media were changed every other day. All experiments were repeated two times and performed in triplicate ($n = 3$).

2.5 MTT assay

SaOS-2 cell proliferation and viability on the scaffolds were quantitatively evaluated via MTT assay [36]. The assay is dependent on the cellular reduction of MTT [3-(4,5-dimethylthialzol-2-yl)-2,5-diphenyltetrazolium bromide], by the mitochondrial dehydrogenase enzymes of viable cells, to a blue formazan product which can be measured by a spectrophotometer. The amount of purple formazan crystals formed is proportional to the number of viable cells. 3, 7, 10, and 14 days after cell seeding, culture medium from each well was aspirated and replaced with 10 µL per well of MTT solution (5 mg/mL in McCoy's medium 5A without serum) for each scaffold in 96-well culture plates. The plate was incubated for 4 h at 37 °C. The media were aspirated and the cells were then lysed using 100 µL per well of dimethylsulfoxide (DMSO) to release and solubilize formazan crystals. After 10 min of rotary agitation, the absorbance of the DMSO solution at 570 nm (690 nm ref.) was measured using a UV/Visible spectrophotometer (Molecular Devices-Versa Max).

The statistical analysis was performed using one-way analysis of variance (ANOVA) method. Post-hoc multiple comparisons of the mean of independent groups were made using Tukey test at statistically significant value, $P < 0.05$.

2.6 Alkaline phosphatase (ALP) activity

ALP activity of the samples after 14 days was measured using a colorimetric ALP Assay Kit (Abcam 83369). ALP catalyzes the hydrolysis of phosphate esters in alkaline buffer and produces an organic radical and inorganic phosphate. The kit is based on this reaction that uses *p*-nitrophenyl phosphate (*p*NPP) as a phosphatase substrate which turns yellow ($\lambda_{max} = 405$ nm) when dephosphorylated by ALP. The cells on the scaffolds were washed with PBS and homogenized in the assay buffer. Homogenates were centrifuged at 13,000×*g* for 3 min to remove insoluble material. 80 µL supernatant was transferred to 96-well plates and 20 µL stop solution was added on each well 20 µL to terminate ALP activity in the sample. 50 µL of the 5 mM *p*NPP solution was added to each well containing the test samples and background controls, and incubate the reaction for 60 min at 25 °C in the dark. The standard curve was prepared by 0, 4, 8, 12, 16, 20 nmol/well *p*NPP standard provided by the manufacturer using the same procedure. OD was measured at 405 nm using a UV/visible spectrophotometer (Molecular Devices-Versa Max), and the ALP activity was calculated by the formula:

$$\text{ALP activity (U/mL)} = \text{A} / \text{V} / \text{T} \quad (1)$$

where A is amount of *p*NPP generated by samples (in µmol), V is the volume of sample added in the assay well (in mL), and T is reaction time (in min). The Unit (U) used in this protocol is Glycine Unit that translates to the amount of enzyme causing the hydrolysis of one micromole of *p*NPP per minute at pH 9.6 and 25 °C (glycine buffer). In order to normalize the results with the cell numbers, the resulting ALP activity was divided by the viable cell absorbance obtained from MTT tests, and ALP activity was graphed as ALP activity per viable cell absorbance.

2.7 Cell morphology

The cell morphology of the SaOS-2 osteoblast-like cells on scaffold surfaces after cell culture for 7 and 14 days was observed using scanning electron microscopy (SEM, JSM-6060 JEOL). The media were aspirated from culture wells, the scaffolds were washed with 0.1 M sodium cacodylate buffer and fixed in 2.5 % glutaraldehyde in 0.1 M sodium cacodylate at 4 °C for 2 h, and post fixed in 1 % osmium tetroxide in 0.1 M cacodylate for 90 min in the dark. Following a buffer rinse, the samples underwent gradual dehydration in an ethanol series. Finally, samples were placed in HMDS for 45 min, allowed to dry overnight, and stored in a desiccator. Samples were sputter-coated with gold–palladium prior to imaging.

2.8 Characterization

Solution conductivity was measured with a conductivity meter (WTW Cond 3110SET1). The effects of different types of surfactants on the surface morphology of the nanocomposite fibers, apatite like mineral formation while incubating in SBF and osteoblastic cellular responses were investigated by SEM. The average diameter of electrospun fibers was estimated from the SEM micrographs via Image J program. For each sample, the fiber diameter was measured at 100 different points. Dispersion and presence of HAp on the fiber surface before mineralization and chemical composition of the minerals formed during biomineralization were investigated by EDS and EDS/Mapping analyses. Fourier transform infrared spectroscopy (FTIR) (Perkin Elmer Spectrum BX) was also used to determine the chemical composition of the nanofibers and apatite like crystals in the wave number range of 500–4,400 cm^{-1} with a resolution of 4 and 25 scans per sample. Determination of the crystal structure of apatite like particles was performed on a Rigaku D/Max. 2200/RC Model X-ray diffractometer (XRD) with Cu–Kα radiation (1.5406 Å) using a 0.05° step size and a 2 s dwell time.

Table 1 Solution conductivities and average diameters of the samples

Sample	Sample code	Solution conductivity (μS/cm)	Average diameter (nm)
%9 PHBV/%2 BTEAC	PHBV	1.7	571 ± 160
%9 PHBV/Nano HAp/%2 BTEAC/%0.2 HSA	PHBV–HSA	1.8	622 ± 129
%9 PHBV/Nano HAp/%2 BTEAC/%0.2 TWEEN20	PHBV–TWEEN20	1.8	822 ± 186
%9 PHBV/Nano HAp/%2 BTEAC/%0.2 SDS	PHBV–SDS	1.5	815 ± 171
%9 PHBV/Nano HAp/%2 BTEAC/%0.2 DOC	PHBV–DOC	1.3	574 ± 138
%9 PHBV/Nano HAp/%2 BTEAC/%0.2 DTAB	PHBV–DTAB	2.9	714 ± 150

All diameters were presented as mean ± standard deviation (SD)

Thermal analyses of the mats before and after biomineralization were performed using a thermogravimetric differential thermal analysis (DTA/TGA) (Shimadzu DTG-60H). Samples were scanned from 25 to 700 °C under a nitrogen atmosphere with a heating rate of 10 °C/min. From the DTA curves, apparent melting (T_m) and decomposition temperatures ($T_{decomp.}$) were estimated and the data for enthalpy of fusion (ΔH_f) of each composite mat was determined from the area under the melting peak. Relative degree of crystallinity, X_c, of the mats were then calculated using the enthalpy of fusion value by the following equation;

$$X_c(\%) = \Delta H_f / (W_{PHBV} \times \Delta H_{ref}) \times 100 \quad (2)$$

where W_{PHBV} is the weight fraction of PHBV in the sample and ΔH_{ref} is the enthalpy of fusion of 100 % crystallized PHBV which is 146 J/g [37].

3 Results

3.1 Nanocomposite fiber production and characterization

The composite solution was prepared from PHBV (9 wt%), HAp (5 wt%), BTEAC (2 wt%) and 0.2 wt% of one of the selected surfactants according to our preliminary studies and a stable suspension was maintained for at least 24 h without any phase separation. Then, the composite suspension was electrospun with the optimized processing parameters (voltage: 20 kV, flow rate: 1 mL/h, distance: 15 cm). For all the processing parameters, the average diameters of the fibers were about 400–1,000 nm (Table 1). Six different types of electrospun fibers obtained from solutions with conductivities ranging from 1.3 to 2.9 μS/cm were coded as shown in Table 1.

Continuous electrospinning was achieved for all samples without any bead formation. SEM images of the HAp/PHBV composite nanofibers containing both one of the listed surfactants and BTEAC are given in Fig. 1. Bright spots due to HAp components were clearly visible at a magnification of 5,000× and Ca/P ratios were found about 1.67 by EDS analysis. Figure 2 shows EDS/Mapping spectra of the HAp/PHBV composite nanofibers. All mapping results revealed uniform distribution of Ca on the PHBV fibers.

3.2 Biomineralization studies

The bone-bonding or calcification ability was evaluated by analyzing apatite formation on the surface of the electrospun mats in SBF solution containing ion concentrations nearly equal to human blood plasma. For the first week of SBF incubation, formation of apatite like minerals was commenced only in PHBV–SDS mat. After 3 weeks in SBF plenty of apatite like minerals nucleated on the surface of PHBV–HSA mat whereas slight amount of mineral clusters were detected on PHBV–DOC mat. Furthermore, as shown in Fig. 3, intense formation of apatite like minerals was observed throughout the PHBV–SDS mat. Even though no apatite formation was detected at the third week of biomineralization on the PHBV–TWEEN20 and PHBV–DTAB mats, increased amount of apatite like mineral clusters was observed at the end of fifth week in biomineralization for all samples. Formation of a continuous layer of apatite like minerals was observed for PHBV–SDS mat and also fibers of PHBV–HSA and PHBV–DTAB mats were completely covered (Fig. 4). No apatite-like mineral formation was observed for PHBV mats as expected indicating that HAp incorporation enhanced the nucleation and adhesion of apatite-like minerals.

3.3 FTIR analysis

The FTIR spectra of all the mats before and after biomineralization showed similar peaks due to PHBV matrix and HAp composition. As the surfactants' quantity was low with respect to polymer concentration, the most intense IR bands of the surfactants could not be detected. FTIR spectra of PHBV–DTAB mat before and after mineralization for

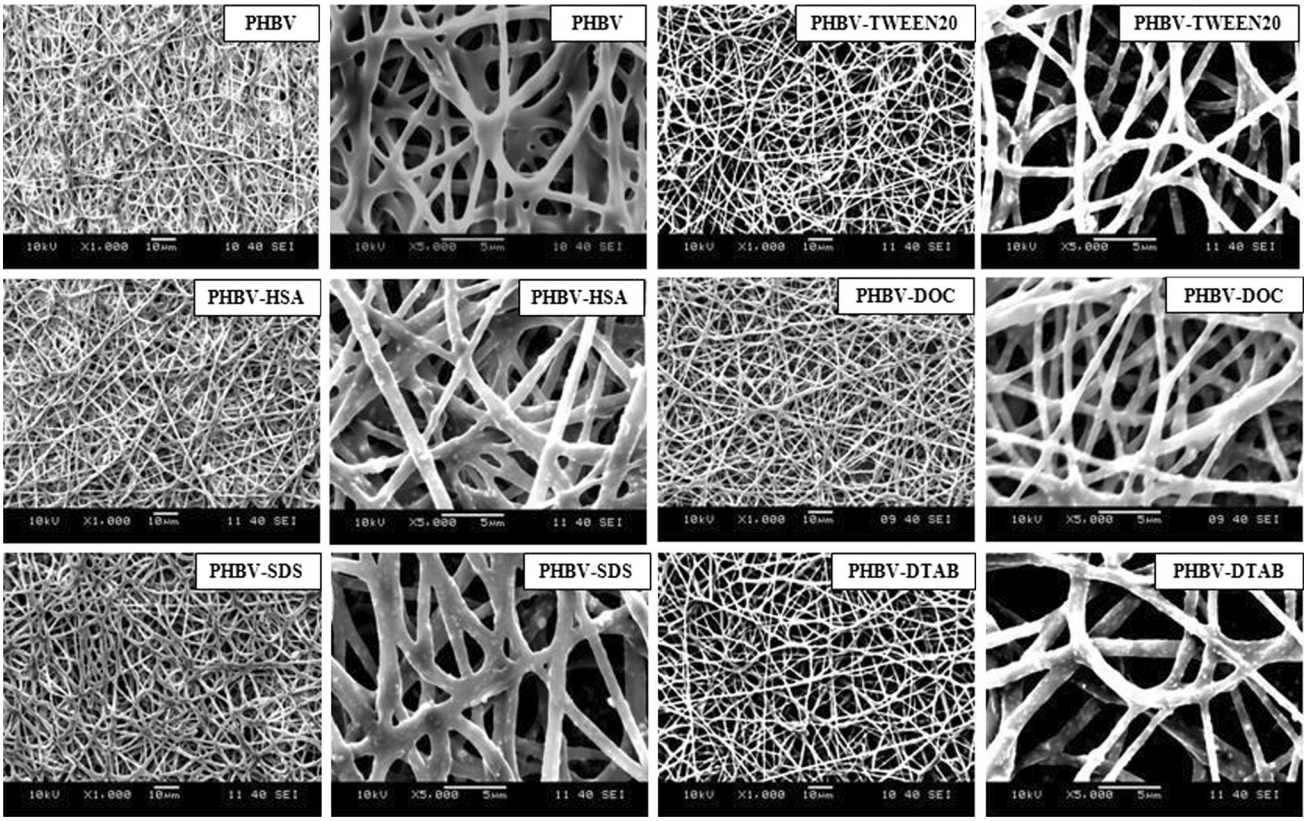

Fig. 1 SEM images of the HAp/PHBV composite fibers at a magnification of 1,000× and 5,000× respectively

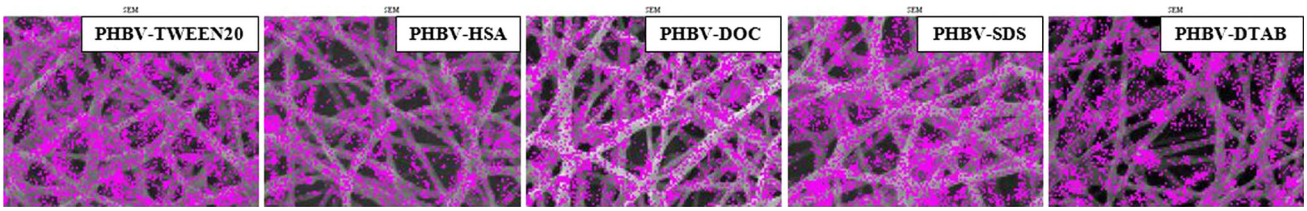

Fig. 2 EDS mapping spectra of HAp/PHBV composite nanofibers where pink spots represent Ca (magnification—5,000×)

5 weeks were given as an example in Fig. 5. C=O stretching vibration of PHBV appeared at 1,726 cm^{-1}, whereas C–O stretching bands were at 1,278 and 1,054 cm^{-1}. C–H stretching bands were at around 2,978 and 2,935 cm^{-1} besides C–H bending vibrations appeared at 1,453 and 1,380 cm^{-1}. New bands of P–O stretching and bending vibrations appeared at 1,200–900 and 700–500 cm^{-1} region respectively due to HAp incorporation into the PHBV matrix. After biomineralization C=O and C–O stretching vibrations of the PHBV matrix showed a sharp decrease in intensity which is an indication of highly dense deposition of HAp. Characteristic peaks of apatite PO_4^{3-} groups showed at 1,016 and 960 cm^{-1} which were assigned to asymmetric and symmetric stretching vibrations respectively. Also, 600 and 560 cm^{-1} bands arose from the P–O bending modes of the phosphate groups.

3.4 XRD analysis

XRD diffraction patterns of PHBV–DTAB mats before and after biomineralization for 5 weeks were given in Fig. 6. Characteristic peaks of PHBV were at $2\theta = 13.6°$, 17.1°, 25.7° (ref 116) where additional peaks related to HAp appeared at $2\theta = 31.7°$, 32.1°, 32.9° (JCPDS no: 00-009-0432) after incubation in SBF.

3.5 Thermal analysis of HAp/PHBV nanocomposite fibers

Thermal properties of the nanocomposite fibers were investigated using DTA/TGA and their apparent melting peak temperature, enthalpy of fusion, theoretical and experimental % crystallinity and polymer decomposition

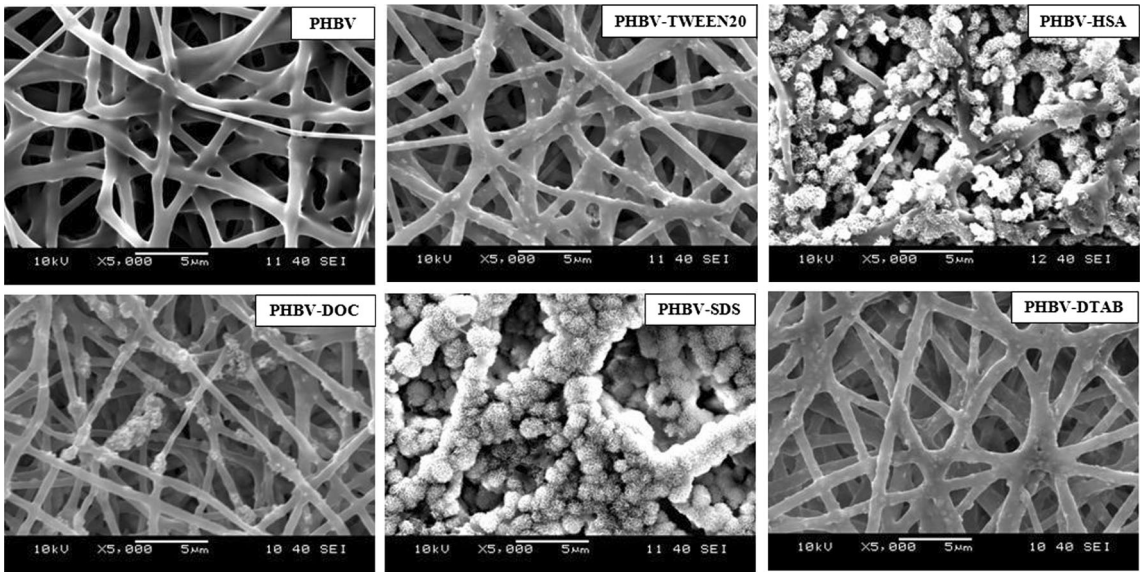

Fig. 3 SEM images of the HAp/PHBV composite nanofibers after incubation in SBF at 37 °C for 3 weeks

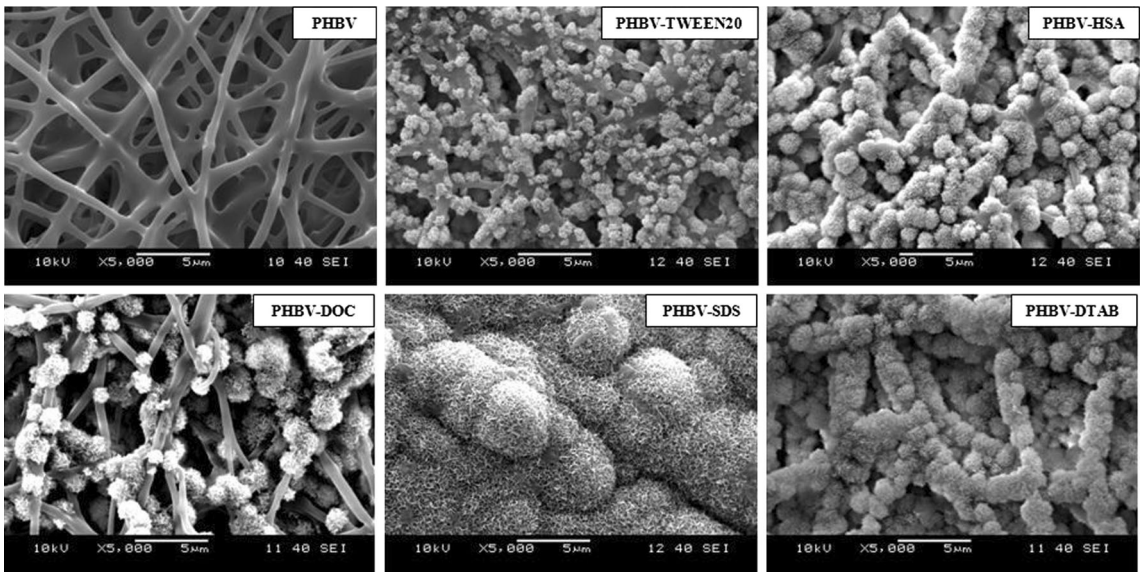

Fig. 4 SEM images of the HAp/PHBV composite nanofibers after incubation in SBF at 37 °C for 5 weeks

temperature data were given in Table 2. The weight fraction of the polymer used to calculate theoretical and experimental percent crystallinities of the mats were determined from the quantities of constituents of the nanocomposite suspension and from the weight loss value obtained from TGA thermograms due to organic fraction, respectively (Table 2). Theoretical and experimental crystallinities of nanocomposite mats exhibited similar values.

Addition of HAp and neutral surfactants, especially TWEEN20, did not significantly influence the crystallinity of nanocomposite mats with respect to PHBV mat. However, addition of ionic surfactants decreased the crystallinity of the mats which might be due to repulsion of the charges decreasing interaction between the polymer chains. Theoretical % crystallinity of PHBV mats decreased from 57.2 to 34.5 after 5 weeks of incubation in SBF. This decrease may induce the degradation of the polymer chains as chain scission can occur in the amorphous part of the scaffold matrix. The fastest mineralized PHBV–SDS mats showed slight change in crystallinity besides slowest mineralized PHBV–DOC and PHBV–TWEEN20 mats resulted in lowest % crystallinity after mineralization (Table 2). It can be claimed that early

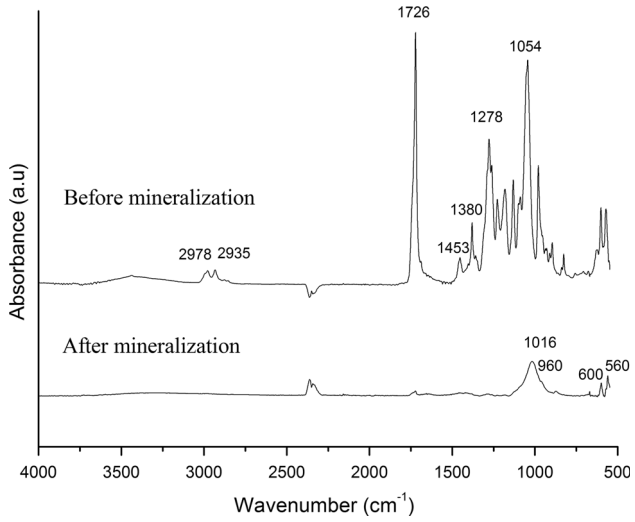

Fig. 5 FTIR spectra of PHBV–DTAB mat before and after mineralization for 5 weeks

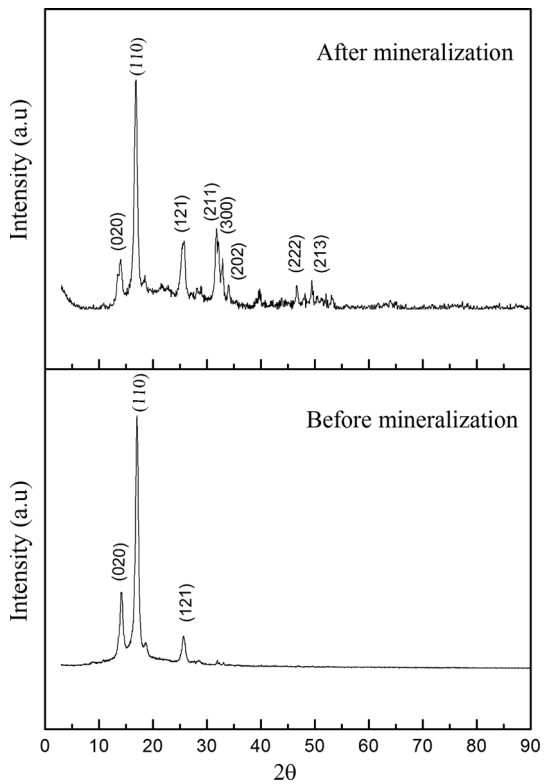

Fig. 6 XRD patterns of PHBV–DTAB mat before and after mineralization for 5 weeks

deposition of minerals on PHBV–SDS mats shields the polymer from SBF solution whereas uncoated regions on the PHBV–DOC and PHBV–TWEEN20 mats surface maintain the interaction between the polymer and SBF solution. In addition, even though PHBV–HSA and PHBV–DTAB mats showed good mineralization in SBF, their % crystallinity values decreased more than PBHV–SDS mat after incubation. These results might be correlated with the slower mineralization rates of these two mats that interacted longer with SBF with respect to PHBV–SDS mat.

Actual weight percentage of HAp in the composite mats and weight gain after incubation were determined from thermal gravimetric analyses. Starting from theoretical 19.3 wt% HAp in all the mats before mineralization, HAp content was increased to 60–70 wt% after 5 weeks of immersion in SBF with no significant change with respect to the surfactant type. The actual weight percentages of HAp were found to be similar to the intended theoretical compositions meaning that HAp was homogenously distributed on the composite nanofibers. Figure 7 shows the TGA thermograms of the PHBV and PHBV–DTAB composite nanofiber mats before and after incubation in SBF for 5 weeks. PHBV and PHBV–DTAB mats were found to contain 3.8 and 20.1 wt% inorganics before mineralization and inorganic contents were 4.4 and 69 wt% after mineralization. No distinct inorganic content change was observed for PHBV mats. These results suggest that incorporation of HAp clearly enhanced the quantity of the deposited minerals on the mats surface.

3.6 MTT assay

The MTT results revealed that all scaffolds favored osteoblastic cell attachment and proliferation (Fig. 8). The cell proliferation increased about fivefold from 3 to 14 days for all types of scaffolds whereas the cells proliferated gradually on the control group.

3.7 ALP activity of cells

ALP activity expressed by SaOS-2 cells seeded on different scaffolds was assessed after 14 days of culture period (Fig. 9). The ALP activity was higher on the PHBV–SDS scaffold compared to PHBV–HSA and PHBV–DTAB, which were still higher than on polystyrene tissue culture plates.

3.8 Cell morphology

After cell culture for up to 14 days, cells on the nanofibrous scaffolds were observed to be spreading well. The cell morphology on the various scaffold surfaces was observed by SEM. Cell growth was evident and cellular morphology was similar regardless of the scaffold type. After 14 days of incubation, the SaOS-2 osteoblast-like cells showed a randomly oriented, well-spread and flattened morphology on all composite mesh surfaces as shown in Fig. 10. They exhibited a polygonal shape with lamellipodia and

Table 2 Thermal properties and apparent crystallinity of HAp/PHBV mats

Sample	T_m (°C)	ΔH_f (J/g)	X_c (%, Before incubation)		X_c (%, After incubation)	T_{decomp}
			Theoretical	Experimental		
PHBV	171.6	80.4	56.3	57.2	34.5	269.3
PHBV–HSA	170.6	57.8	51.4	52.1	36.1	256.3
PHBV–TWEEN20	171.5	66.2	58.9	57.0	28.6	258.6
PHBV–SDS	173.4	52.7	46.9	47.2	41.6	236.4–273.3
PHBV–DOC	164.3	56.9	50.6	47.7	31.6	232.1
PHBV–DTAB	163.6	50.5	46.9	47.2	37.2	262.9

T_m apparent melting peak temperature, ΔH_f apparent enthalpy of fusion, X_c crystallinity index, T_{decomp} decomposition temperature of polymer

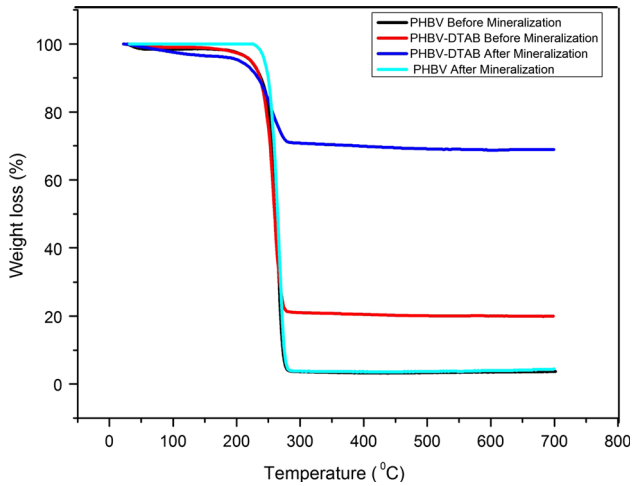

Fig. 7 TGA curves of PHBV and PHBV–DTAB mats before and after mineralization for 5 weeks

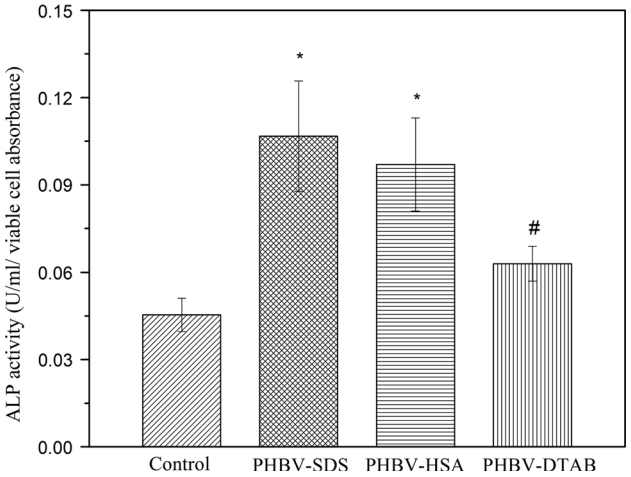

Fig. 9 ALP expression by SaOS-2 cells seeded on different scaffolds after 14 days of culture period (data are expressed as mean ± SD; $n = 3$, * $P < 0.05$, # $P < 0.01$)

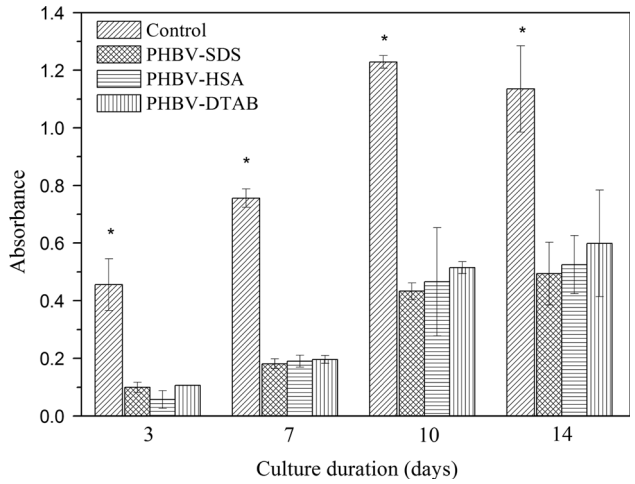

Fig. 8 Cell viability on PHBV–DTAB, PHBV–HSA and PHVB–SDS scaffolds after 3, 7, 10, and 14 days of culture. The experiment was repeated two times and in triplicate ($n = 3$) for each sample. Data are shown as averages with the *error bars* indicating standard deviation, * $P < 0.05$

filopodia that reached into the interspaces between the nanofibers, indicating a good interconnection between the cells and the nanofibers.

4 Discussion

The development of PHBV nanofibers with HAp via electrospinning has enhanced the scope of fabricating scaffolds that mimic the architecture of natural bone tissue. However, HAp, as a hydrophilic ceramic powder, shows low affinity to organic solvents which results in ceramic agglomerates within polymers [26]. Therefore, in order to obtain continuous and uniform ceramic-filled biocomposite fibers, surfactants were used as a mediator between the hydrophilic HAp and hydrophobic PHBV in chloroform. Also, BTEAC was used as an organosoluble salt to help improving the electro-spinnability of the composite suspension as well as the morphological uniformity of the HAp/PHBV composite fibers (Figs. 1, 2). One of the

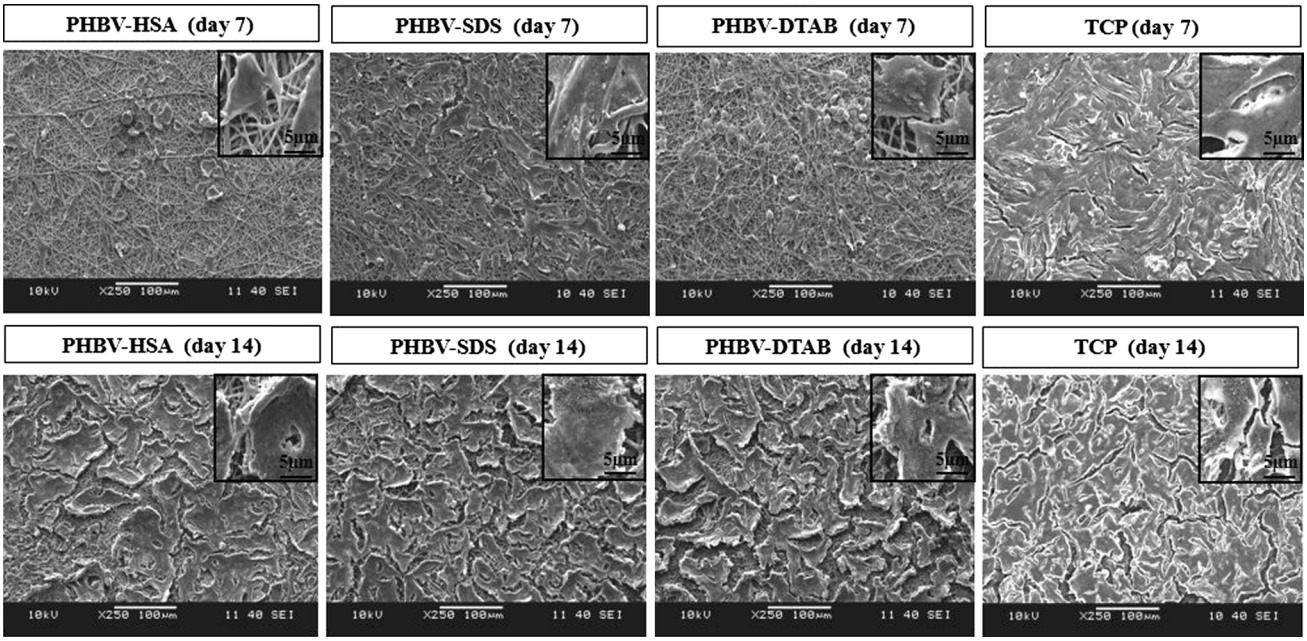

Fig. 10 SEM images of osteoblast cell (SaOS-2) adhesion and spreading on (a) PHBV–HSA, (b) PHBV–SDS, (c) PHBV–DTAB mats after 7 and 14 days of culture

disadvantages of using salt is that; salt addition decreases stability of the suspensions. However, addition of salts increases the charge density in ejected jets and thus, stronger elongation forces are imposed to the jets due to self repulsion of excess charges under the electrical field resulting in smaller diameter of electrospun fibers [38–40]. Therefore, the amount of salt added was finely tuned and the order of addition of the constituents was significant so as to retain the stability of the composite suspension.

Biomineralization on scaffolds in SBF has been regarded as evidence for the in vitro bioactivity of materials [32]. It has been shown previously that CaP coating on different metal implants and polymers increase proliferation rate of osteoblastic cells. CaP coatings are applied on orthopaedic implants particularly to enhance initial fixation and improve osseointegration [41]. CaP coatings were also shown to enhance human bone marrow-derived mesenchymal cells' differentiation to osteogenic lineage (e.g. osteopontin and osteonectin) and osteoblast synthetic activity (e.g. ALP activity, collagen type I) [41]. Similarly, polymer/CaP composite scaffolds have been shown to increase in vitro bone ECM formation and mineralization compared to scaffolds without a biomimetic CaP component [42–44]. Osteoblasts are involved in bone metabolism and participate in calcium/phosphate homeostasis. Therefore existence of calcium ions in their microenvironment could enhance osteoblasts' proliferation and expression of phenotype [45–47].

Intrinsic osteoconductivity of apatite minerals can also be attributed to their high protein adsorption capacity, particularly adhesion proteins such as fibronectin and vitronectin from the serum. The adsorption of proteins on biomaterial surfaces is a complex process, and requires that the proteins to retain their bioactive conformation upon contact with the surface [48–52]. Initial adhesion of cells is primarily influenced by the binding of integrins on the cell surface to these adhesion molecules. Integrin binding generates intracellular signals that affect cell cytoskeletal organization and in turn spreading and subsequent cellular responses [42, 53].

Material surface physico-chemical properties are the dominant factors influencing cellular adhesion, spreading and proliferation on a biomaterial surface [34, 54–56]. Nanofibers provide a high surface area-to-volume ratio that triggers cell attachment and growth and enhance tissue regeneration when compared with other types of scaffold microstructures. Cell attachment is the first phase of cell–material interactions and influences the growth, morphology, proliferation and differentiation of a cell. Highly porous and interconnected nanofibrous microstructure provided by electrospinning is rather favorable for tissue engineering applications, particularly for anchorage dependent cells such as osteoblasts [1, 3, 43, 57]. Besides good cell anchorage, this specific microstructure also furnish space for vascular ingrowth to provide optimal nutrient and oxygen transport to the tissue-engineered bone [58, 59]. Our SEM observations indicate that the osteoblasts show a flat form extended in all directions and they have strong binding and affinity to all nanofibrous surfaces

(Fig. 10). Polygonal shape is characteristic for osteoblastic lineage [54, 59]. This shows good biocompatibility and favorable properties for osteoblastic cell growth.

Polarity and surface energy is another major factor regulating cell behavior [60, 61]. Surfaces with enhanced polarity are shown to promote the attachment of chondrocytes [62], osteoblasts [63], and fibroblasts [64]. Barber and coauthors [65] stated that molecular reorientation of functional groups towards or away from electrospun fiber surfaces can be controlled using different applied voltage polarities during electrospinning so that polar groups that are mobile inside the electrospinning liquid jet will orient relatively to the applied voltage charge. When the mineralization rates of the mats were compared, PHBV–SDS mat was by far the fastest one, followed by PHBV–HSA and PHBV–DTAB mats (Fig. 4). We believe that electrospinning with a positive voltage caused orientation of anionic surfactant SDS carrying HAp towards the nanofiber surface better than the mat with a neutral or positively charged surfactant producing denser preferential sites for nucleation of apatite-like crystals. However, slow nucleation and growth of crystals on the PHBV–DOC and PHBV–TWEEN20 mats could be due to rigid steroidal structure of the negatively charged surfactant DOC and branched structure of neutral surfactant TWEEN20 containing ethylene oxide side chains, respectively, limiting these surfactants' mobility towards the fiber surface during the electrospinning process. It is evident from our results that use of anionic SDS surfactant improved biomineralization on the fiber surfaces in SBF. This is supported by the increased osteoblastic metabolic activity determined by ALP on these surfaces (Figs. 8, 9). The natural life cycle of an osteoblastic cell includes a proliferation period coupled with some collagen production while phenotypic protein expression is not substantial. This is followed by a period of increased ALP expression, among other proteins, indicating maturation. In natural bone remodeling, ALP is involved in preparation of the ECM for deposition of mineral. Therefore it is commonly used as a marker of osteoblastic maturation [42, 54, 66, 67]. Higher ALP activity on PHBV–SDS scaffold is parallel with the higher biomineralisation rate on this scaffold. It was stated in the literature that incorporation of HAp in polymer based scaffolds increases ALP activity which is an early osteogenic marker for differentiation and it is important for the construction of bone matrix [68]. It is also noteworthy from the results that there is an inverse proportion between the cell proliferation and ALP activity data. Oven et al. [69] observed a reciprocal relationship between the decrease in cell proliferation and the subsequent induction of bone cell differentiation expressed by increased ALP activity. Therefore, PHBV–SDS mat with the highest ALP activity value and lowest cell number seems to be related to earlier progression of differentiation compared to other mats. Several rat, mouse, and human osteoblastic cell lines including SaOS-2 were reported to carry calcium-sensing receptors (CaR) causing them to respond to extracellular calcium by proliferating and maturation [70–72]. In human body, the level of Ca^{2+} beneath a resorbing osteoclast reaches 40 mM [73]. High levels of extracellular Ca^{2+} may also provide osteoblastic cells an indication of ongoing bone resorption, therefore triggering differentiation to maintain the balance between bone resorption and formation.

Our experimental results show that osteoblastic adhesion and proliferation, as well as ALP metabolic activity has been mainly influenced by HAp deposition (biomineralization) rather than scaffold microstructure, because all the scaffold surfaces had a similar morphological topography with non-woven nanofibrous mashes.

5 Conclusion

Continuous and uniform HAp/PHBV composite nanofibers were successfully generated within a diameter range of 400–1,000 nm by the mediation of all surfactant types. The experimental results showed that incorporation of HAp with any of the surfactants activates the precipitation rate of the apatite-like particles which in turn affects the percent crystallinity of the composite nanofibers in SBF. However, mineralization was greatly enhanced on the fibers produced with the aid of flexible surfactants DTAB, HSA, and especially SDS that are capable of carrying HAp towards the nanofiber surface on where also osteoblastic metabolic activity was similarly increased. The produced HAp/PHBV nanofibrous composite scaffolds would be a promising candidate as an osteoconductive bioceramic/polymer composite material for tissue engineering applications.

Acknowledgments A. Suslu acknowledges the support from TUBITAK, in the framework of the National Scholarship Programme for PhD Students.

References

1. Jang JH, Castano O, Kim HW. Electrospun materials as potential platforms for bone tissue engineering. Adv Drug Deliv Rev. 2009;61:1065–83.
2. Lü LX, Wang YY, Mao X, Xiao ZD, Huang NP. The effects of PHBV electrospun fibers with different diameters and orientations on growth behavior of bone-marrow derived mesenchymal stem cells. Biomed Mater. 2012;7:1–11.
3. Pham QP, Sharma U, Mikos AG. Electrospinning of polymeric nanofibers for tissue engineering applications: a review. Tissue Eng. 2006;12(5):1197–211.
4. Li WJ, Laurencin CT, Caterson EJ, Tuan RS, Ko FK. Electrospun nanofibrous structure: a novel scaffold for tissue engineering. J Biomed Mater Res. 2002;60:613–21.

5. Smith IO, Liu XH, Smith LA, Ma PX. Nano-structured polymer scaffolds for tissue engineering and regenerative medicine. Nanomed Nanobiotechnol. 2009;1(2):226–36.
6. O'Brien FJ. Biomaterials & scaffolds for tissue engineering. Mater Today. 2011;14(3):88–95.
7. Xie J, Li X, Xia Y. Putting electrospun nanofibers to work for biomedical research. Macromol Rapid Commun. 2008;29:1775–92.
8. Song JH, Kim HE, Kim HW. Electrospun fibrous web of collagen–apatite precipitated nanocomposite for bone regeneration. J Mater Sci Mater Med. 2008;19:2925–32.
9. Sui G, Yang X, Mei F, Hu X, Chen G, Deng X, Ryu S. Poly-L-lactic acid/hydroxyapatite hybrid membrane for bone tissue regeneration. J Biomed Mater Res. 2007;82A:445–54.
10. Ma PX. Scaffolds for tissue fabrication. Mater Today. 2004;7(5):30–40.
11. Christenson EM, Anseth KS, Beucken JJ, Chan CK, Ercan B, Jansen JA, Laurencin CT, Li WJ, Murugan R, Nair LS, Ramakrishna S, Tuan RS, Webster TJ, Mikos AG. Nanobiomaterial applications in orthopedics. J Orthop Res. 2007;25(1):11–22.
12. Smith LA, Liu X, Ma PX. Tissue engineering with nano-fibrous scaffolds. Soft Matter. 2008;4:2144–9.
13. Holzwartha JM, Ma PX. 3D nanofibrous scaffolds for tissue engineering. J Mater Chem. 2011;21:10243–51.
14. Smith LA, Ma PX. Nano-fibrous scaffolds for tissue engineering. Colloids Surf B Biointerfaces. 2004;39:125–31.
15. Meng W, Xing ZC, Jung KH, Kim SY, Yuan J, Kang IK, Yoon SC, Shin HI. Synthesis of gelatin-containing PHBV nanofiber mats for biomedical application. J Mater Sci Mater Med. 2008;19:2799–807.
16. Sill TJ, Recum HA. Electrospinning: applications in drug delivery and tissue engineering. Biomaterials. 2008;29:1989–2006.
17. Agarwal S, Wendorff JH, Greiner A. Use of electrospinning technique for biomedical applications. Polymer. 2008;49:5603–21.
18. Rezwan K, Chen QZ, Blaker JJ, Boccaccini AR. Biodegradable and bioactive porous polymer/inorganic composite scaffolds for bone tissue engineering. Biomaterials. 2006;27:3413–31.
19. Armentano I, Dottori M, Fortunati E, Mattioli S, Kenny JM. Biodegradable polymer matrix nanocomposites for tissue engineering: a review. Polym Degrad Stab. 2010;95:2126–46.
20. Kim HW, Song JH, Kim HE. Nanofiber generation of gelatin/hydroxyapatite biomimetics for guided tissue regeneration. Adv Funct Mater. 2005;15:1988–94.
21. Nair LS, Laurencin CT. Biodegradable polymers as biomaterials. Prog Polym Sci. 2007;32:762–98.
22. Hong Z, Qiu X, Sun J, Deng M, Chen X, Jing X. Grafting polymerization of L-lactide on the surface of hydroxyapatite nano-crystals. Polymer. 2004;45:6699–706.
23. Xu X, Chen X, Liu A, Hong Z, Jing X. Electrospun poly(L-lactide)-grafted hydroxyapatite/poly(L-lactide) nanocomposite fibers. Eur Polym. 2007;43:3187–96.
24. Fujihara K, Kotaki M, Ramakrishna S. Guided bone regeneration membrane made of polycaprolactone/calcium carbonate composite nano-fibers. Biomaterials. 2005;26:4139–47.
25. Venugopal J, Vadgama P, SampathKumar TS, Ramakrishna S. Biocomposite nanofibres and osteoblasts for bone tissue engineering. Nanotechnology. 2007;18:1–8.
26. Kim HW, Lee HH, Knowles JC. Electrospinning biomedical nanocomposite fibers of hydroxyapaite/poly(lactic acid) for bone regeneration. J Biomed Mater Res A. 2006;79(3):643–9.
27. Ito Y, Hasuda H, Kamitakahara M, Ohtsuki C, Tanihara M, Kang IK, Kwon OH. A composite of hydroxyapatite with electrospun biodegradable nanofibers as a tissue engineering scaffold. J Biosci Bioeng. 2005;100(1):43–9.
28. Sultana N, Wang M. Fabrication of HA/PHBV composite scaffolds through the emulsion freezing/freeze-drying process and characterisation of the scaffolds. J Mater Sci Mater Med. 2008;19:2555–61.
29. Sultana N, Wang M. PHBV/PLLA-based composite scaffolds fabricated using an emulsion freezing/freeze-drying technique for bone tissue engineering: surface modification and in vitro biological evaluation. Biofabrication. 2012;4:1–15.
30. Ndreu A, Nikkola L, Ylikauppila H, Ashammak N, Hasirci V. Electrospun biodegradable nanofibrous mats for tissue engineering. Nanomedicine. 2008;3(1):45–60.
31. Cool SM, Kenny B, Wu A, Nurcombe V, Trau M, Cassady AI, Grøndahl L. Poly(3-hydroxybutyrate-co-3-hydroxyvalerate) composite biomaterials for bone tissue regeneration: in vitro performance assessed by osteoblast proliferation, osteoclast adhesion and resorption, and macrophage proinflammatory response. J Biomed Mater Res. 2007;82A:599–610.
32. Kokubo T, Takadama H. How useful is SBF in predicting in vivo bone bioactivity? Biomaterials. 2006;27:2907–15.
33. Saha N, Dubey AK, Basu B. Cellular proliferation, cellular viability, and biocompatibility of HA-ZnO composites. J Biomed Mater Res B. 2012;100(1):256–64.
34. Chen X, Li Y, Hodgson PD, Wen C. In vitro behavior of human osteoblast-like cells (SaOS2) cultured on surface modified titanium and titanium–zirconium alloy. Mater Sci Eng C. 2011;31:1545–52.
35. Wang XJ, Li YC, Xiong JY, Hodgson PD, Wen CE. Porous TiNbZr alloy scaffolds for biomedical applications. Acta Biomater. 2009;5(9):3616–24.
36. Mosmann T. Rapid colorimetric assay for cellular growth and survival: application to proliferation and cytotoxicity assays. J Immunol Methods. 1983;65:55–63.
37. Cheng ML, Sun YM. Relationship between free volume properties and structure of poly(3-hydroxybutyrate-co-3-hydroxyvalerate) membranes via various crystallization conditions. Polymer. 2009;50:5298–307.
38. Choi JS, Lee SW, Jeong L, Bae SH, Min BC, Youk JH, Park WH. Effect of organosoluble salts on the nanofibrous structure of electrospun poly(3-hydroxybutyrate-co-3-hydroxyvalerate). Int J Biol Macromol. 2004;34:249–56.
39. You Y, Lee SJ, Min BM, Park WH. Effect of solution properties on nanofibrous structure of electrospun poly(lactic-co-glycolic acid). J Appl Polym Sci. 2006;99:1214–21.
40. Lin K, Chua KN, Christopherson GT, Lim S, Mao HQ. Reducing electrospun nanofiber diameter and variability using cationic amphiphiles. Polymer. 2007;48:6384–94.
41. Wang XJ, Li YC, Hodgson PD, Wen CE. Biomimetic modification of porous TiNbZr alloy scaffold for bone tissue engineering. Tissue Eng A. 2010;16(1):309–16.
42. Sendemir-Urkmez A, Jamison RD. The addition of biphasic calcium phosphate to porous chitosan scaffolds enhances bone tissue development in vitro. J Biomed Mater Res A. 2007;81(3):624–33.
43. Prabhakaran MP, Venugopal J, Ramakrishna S. Electrospun nanostructured scaffolds for bone tissue engineering. Acta Biomater. 2009;5(8):2884–93.
44. Zhang YZ, Venugopal JR, El-Turki A, Ramakrishna S, Su B, Lim CT. Electrospun biomimetic nanocomposite nanofibers of hydroxyapatite/chitosan for bone tissue engineering. Biomaterials. 2008;29(32):4314–22.
45. Duncan RL, Akanbi KA, Farach-Carson MC. Calcium signals and calcium channels in osteoblastic cells. Semin Nephrol. 1998;18:178–90.
46. Dvorak MM, Riccardi D. Ca^{2+} as an extracellular signal in bone. Cell Calcium. 2004;35:249–55.
47. Maeno S, Niki Y, Matsumoto H, Morioka H, Yatabe T, Funayama A, Toyama Y, Taguchi T, Tanaka J. The effect of calcium ion concentration on osteoblast viability, proliferation and

differentiation in monolayer and 3D culture. Biomaterials. 2005;26:455–84.
48. Kilpadi KL, Chang PL, Bellis SL. Hydroxylapatite binds more serum proteins, purified integrins, and osteoblast precursor cells than titanium or steel. J Biomed Mater Res. 2001;57(2):258–67.
49. Yu HS, Jang JH, Kim TI, Lee HH, Kim HW. Apatite-mineralized polycaprolactone nanofibrous web as a bone tissue regeneration substrate. J Biomed Mater Res A. 2009;88(3):747–54.
50. Chou YF, Huang W, Dunn JC, Miller TA, Wu BM. The effect of biomimetic apatite structure on osteoblast viability, proliferation, and gene expression. Biomaterials. 2005;26(3):285–95.
51. Ko EK, Jeong SI, Rim NG, Lee YM, Shin H, Lee BK. In vitro osteogenic differentiation of human mesenchymal stem cells and in vivo bone formation in composite nanofiber meshes. Tissue Eng A. 2008;14:2105–19.
52. Whited BM, Whitney JR, Hofmann MC, Xu Y, Rylander MN. Pre-osteoblast infiltration and differentiation in highly porous apatite-coated PLLA electrospun scaffolds. Biomaterials. 2011;32(9):2294–304.
53. Degasne I, Baslé MF, Demais V, Huré G, Lesourd M, Grolleau B, Mercier L, Chappard D. Effects of roughness, fibronectin and vitronectin on attachment, spreading, and proliferation of human osteoblast-like cells (Saos-2) on titanium surfaces. Calcif Tissue Int. 1999;64:499–507.
54. Anselme K. Osteoblast adhesion on biomaterials. Biomaterials. 2000;21(7):667–81.
55. Wei J, Heo SJ, Kim DH, Kim SE, Hyun YT, Shin JW. Comparison of physical, chemical and cellular responses to nano- and microsized calcium silicate/poly(epsilon-caprolactone) bioactive composites. J R Soc Interface. 2008;5:617–30.
56. Osathanon T, Bespinyowong K, Arksornnukit M, Takahashi H, Pavasant P. Human osteoblast-like cell spreading and proliferation on Ti–6Al–7Nb surfaces of varying roughness. J Oral Sci. 2011;53:23–30.
57. Lutolf MP, Hubbell JA. Synthetic biomaterials as instructive extracellular microenvironments for morphogenesis in tissue engineering. Nat Biotechnol. 2005;23(1):47–55.
58. Xu C, Inai R, Kotaki M, Ramakrishna S. Electrospun nanofiber fabrication as synthetic extracellular matrix and its potential for vascular tissue engineering. Tissue Eng. 2004;10:1160–8.
59. Aoki N, Akasaka T, Watari F, Yokoyama A. Carbon nanotubes as scaffolds for cell culture and effect on cellular functions. Dent Mater J. 2007;26(2):178–85.
60. Hallab N, Bundy K, O'Connor K, Moses RL, Jacobs JJ. Evaluation of metallic and polymeric biomaterial surface energy and surface roughness characteristics for directed cell adhesion. Tissue Eng. 2001;71:55–71.
61. Satriano C, Carnazza S, Guglielmino S, Marletta G. Surface free energy and cell attachment onto ion-beam irradiated polymer surfaces. Nucl Instrum Methods Phys Res B. 2003;208:287–93.
62. Lin Y, Wang L, Zhang P, Wang X, Chen X, Jing X, Su Z. Surface modification of poly(L-lactic acid) to improve its cytocompatibility via assembly of polyelectrolytes and gelatin. Acta Biomater. 2006;2:155–64.
63. Schneider GB, English A, Abraham M, Zaharias R, Stanford C, Keller J. The effect of hydrogel charge density on cell attachment. Biomaterials. 2004;25:3023–8.
64. Choee JH, Lee SJ, Lee SJ, Lee YM, Rhess JM, Lee HB, Khang G. Proliferation rate of fibroblast cells on polyethylene surfaces with wettability gradient. J Appl Polym Sci. 2004;92:599–606.
65. Stachewicz U, Stone CA, Willis CR, Barber AH. Charge assisted tailoring of chemical functionality at electrospun nanofiber surfaces. J Mater Chem. 2012;22:22935–41.
66. Di-Silvio L, Gurav N. Osteoblasts. In: Koller MR, Palsson BO, Masters JRW, Koller MR, Palsson BO, Masters JRW, editors. Primary mesenchymal cells. Norwell, MA: Kluwer Academic Publishers; 2001. p. 221–41.
67. Lian JB, Stein GS. Concepts of osteoblast growth and differentiation—basis for modulation of bone cell-development and tissue formation. Crit Rev Oral Biol. 1992;3:269–305.
68. Ngiam M, Liao S, Patil AJ, Cheng Z, Chan CK, Ramakrishna S. The fabrication of nano-hyroxyapatite on PLGA and PLGA/collagen nanofibrous composite scaffolds and their effects in osteoblastic behaviour for bone tissue engineering. Bone. 2009;45:4–16.
69. Owen TA, Aronow M, Shalhoub V, Barone LM, Wilming L, Tassinari MS, Kennedy MB, Pockwinse S, Lian JB, Stein GS. Progressive development of the rat osteoblast phenotype in vitro: reciprocal relationships in expression of genes associated with osteoblast proliferation and differentiation during formation of the bone extracellular matrix. J Cell Physiol. 1990;143(3):420–30.
70. House MG, Kohlmeier L, Chattopadhyay N, Kifor O, Yamaguchi T, Leboff MS, Glowacki J, Brown EM. Expression of an extracellular calcium-sensing receptor in human and mouse bone marrow cells. J Bone Miner Res. 1997;12:1959–70.
71. Ye CP, Yamaguchi T, Chattopadhyay N, Sanders JL, Vassilev PM, Brown EM. Extracellular calcium-sensing-receptor (Car)-mediated opening of an outward K+ channel in Murine Mc3T3-E1 osteoblastic cells: evidence for expression of a functional car. Bone. 2000;27:21–7.
72. Eklou-Kalonji E, Denis I, Lieberherr M, Pointillart A. Effects of extracellular calcium on the proliferation and differentiation of porcine osteoblasts in vitro. Cell Tissue Res. 1998;292:163–71.
73. Silver IA, Murrills RJ, Etherington DJ. Microelectrode studies on the acid microenvironment beneath adherent macrophages and osteoclasts. Exp Cell Res. 1988;175:266–76.